Cell Host & Microbe
Article

Mycobacterium tuberculosis-Driven Targeted Recalibration of Macrophage Lipid Homeostasis Promotes the Foamy Phenotype

Varshneya Singh,[1] Shilpa Jamwal,[1] Ritu Jain,[1] Priyanka Verma,[2] Rajesh Gokhale,[2,3] and Kanury V.S. Rao[1,*]
[1]Immunology Group, International Centre for Genetic Engineering and Biotechnology, Aruna Asaf Ali Marg, New Delhi 110067, India
[2]National Institute of Immunology, Aruna Asaf Ali Marg, New Delhi 110067, India
[3]Institute of Genomics and Integrative Biology, Mall Road, New Delhi 110007, India
*Correspondence: kanury@icgeb.res.in
http://dx.doi.org/10.1016/j.chom.2012.09.012

SUMMARY

Upon infection, *Mycobacterium tuberculosis* (Mtb) metabolically alters the macrophage to create a niche that is ideally suited to its persistent lifestyle. Infected macrophages acquire a "foamy" phenotype characterized by the accumulation of lipid bodies (LBs), which serve as both a source of nutrients and a secure niche for the bacterium. While the functional significance of the foamy phenotype is appreciated, the biochemical pathways mediating this process are understudied. We found that Mtb induces the foamy phenotype via targeted manipulation of host cellular metabolism to divert the glycolytic pathway toward ketone body synthesis. This dysregulation enabled feedback activation of the anti-lipolytic G protein-coupled receptor GPR109A, leading to perturbations in lipid homeostasis and consequent accumulation of LBs in the macrophage. ESAT-6, a secreted Mtb virulence factor, mediates the enforcement of this feedback loop. Finally, we demonstrate that pharmacological targeting of pathways mediating this host-pathogen metabolic crosstalk provides a potential strategy for developing tuberculosis chemotherapy.

INTRODUCTION

Macrophages infected by *Mycobacterium tuberculosis* (Mtb) acquire a "foamy" phenotype that is characterized by the intracellular accumulation of lipid bodies (LBs) (Russell et al., 2009). Mtb-containing phagosomes migrate toward these LBs and, eventually, engulf them (Peyron et al., 2008). This allows for release of bacilli into the LBs, which then serve as a source of nutrients in the form of fatty acids. Additionally, bacilli engulfed within LBs also slow down their replication and concomitantly acquire phenotypic resistance to at least two frontline drugs, rifampicin and isoniazid (Daniel et al., 2011). Thus, foamy macrophages (FMs) form a secure reservoir for the tubercle bacilli and facilitate their persistence in the human host (Peyron et al., 2008).

While the functional significance of FM differentiation in Mtb infection is now better appreciated, the biochemical pathways mediating this process are not known. The present study was therefore initiated to explore this aspect. We found that in infected macrophages, LB accumulation was induced by the pathogen through modulation of lipolysis of neutral lipids. This effect was mediated through recruitment of a feedback loop involving a Gi protein-coupled receptor (GiPCR). Infection of macrophages with Mtb initiated biosynthesis and secretion of the agonist ligand for this GiPCR. The resultant triggering of the receptor then influenced lipolysis by modulating the cAMP-dependent signaling pathway. Notably, activation of this feedback loop was specific to virulent strains of Mtb with the resultant LB formation then shifting the homeostatic balance in favor of inhibition of autophagy and lysosome acidification. Importantly, targeting the Mtb-activated LB accumulation pathway in the host macrophage also provided an approach for the chemotherapy of infections with both drug-sensitive and drug-resistant strains of Mtb.

RESULTS

Mtb-Induced LB Formation Facilitates Attenuation of Host Cellular Microbicidal Activities

THP-1 cells were infected with either the avirulent strain H37Ra or its virulent counterpart H37Rv and then scored for the formation of LBs. While a moderate level of accumulation was seen in H37Ra-infected cells, the extent was significantly greater in cells infected with H37Rv (Figure 1A). This distinction correlated well with findings that in comparison with H37Ra, infection with H37Rv resulted in a near 2-fold increase in triacylglyceride (TAG) levels in the host macrophage (Figure 1B). Further, as earlier described (Peyron et al., 2008), enhanced LB accumulation also inhibited the ability of H37Rv-infected cells to develop a respiratory burst (Figure 1C).

Although autophagy provides an efficient mechanism by which macrophages can eliminate intracellular Mtb, virulent strains actively suppress this pathway (Shin et al., 2010). Interestingly, autophagy has also been implicated in feedback regulation of lipid homeostasis in cells. Whereas basal autophagy mediates lipid turnover, an increase in the pool size of intracellular lipid stores inhibits this process (Singh et al., 2009). This observation hinted that LB formation could additionally serve the pathogen, by inhibiting activation of autophagic pathways. To test this, we compared the intracellular fate of H37Rv under conditions where LB formation was either left unperturbed or

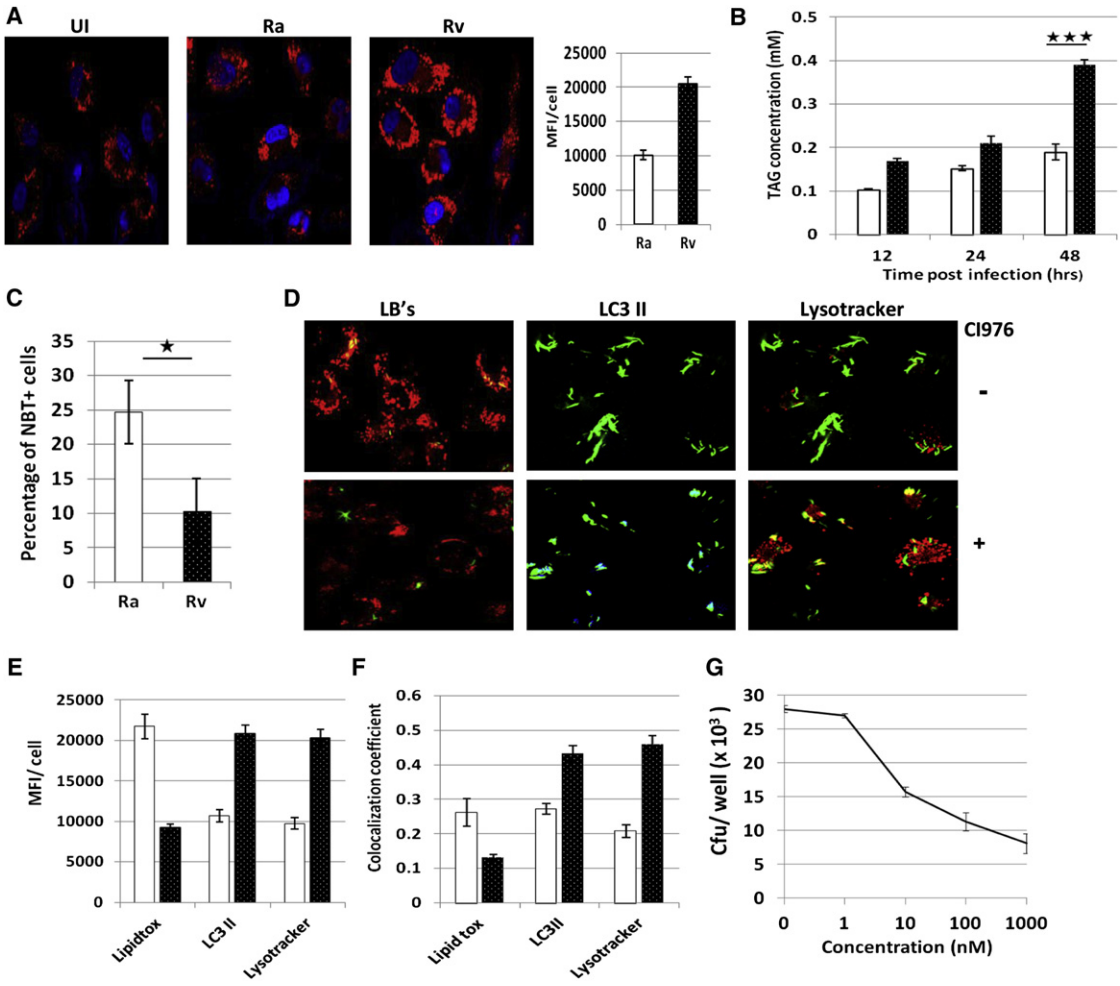

Figure 1. Intracellular Survival of Mtb Depends upon Its Ability to Induce LB Formation in Macrophages

(A) PMA-differentiated THP-1 cells were left uninfected or were infected either with H37Ra or H37Rv and then stained with Lipid Tox (red) at 48h p.i. to score for lipid body formation. Cell nuclei were counterstained with DAPI (blue). The mean fluorescence intensity (MFI)/cell obtained for H37Rv and H37Ra-infected cells are shown in the extreme right panel as relative fluorescence units (rfu). The rfu for uninfected cells was 9800 ± 600. Values are the mean ± SE obtained from at least 50 cells.

(B) Time-dependent increase in TAG levels in H37Rv- (filled bars), versus H37Ra-infected (open bars) cells. Values are the mean ± SD of three experiments (significance ***$p \leq 0.001$).

(C) The effect of H37Ra versus H37Rv infection on the ability of THP-1 cells to activate a respiratory burst is shown (n = 3; mean ± SD, significance, *$p \leq 0.05$).

(D) THP-1 cells were infected with GFP-tagged H37Rv and were either left untreated (–) or treated with the ACAT inhibitor CI976, 100 nM (+) at 6 hr p.i. At 48 hr, the cells were analyzed by confocal microscopy to determine the extent of mycobacterial (green) colocalization with either LBs, autophagosomes/LC3 II (blue), or acidified lysosomes (red).

(E and F) A quantitative representation of the effects of absence (open bars) or presence (filled bars) of CI976 on these three components in terms of MFI/cell (E) and extent of H37Rv colocalization with each of these (F) are shown. Values are the mean ± SE obtained from at least 50 cells.

(G) Dose-dependent effect of CI976 treatment on intracellular bacillary load in H37Rv-infected THP-1 cells. Data shown are from one of two experiments where values are the mean (±SEM) of triplicate wells.

See also Figure S1.

was inhibited with CI-976, an inhibitor of Acyl-CoA cholesterol acyltransferases (ACAT1 and ACAT2), which regulate LB biogenesis by catalyzing the synthesis of cholesteryl esters (Krause et al., 1993).

In the absence of the inhibitor, the bacilli were largely colocalized with LBs by 48 hr postinfection (p.i.) (Figure 1D, upper-left panel; Figure S1 available online). Barely detectable staining was obtained either for the autophagy marker LC3-II (Figure 1D, upper-middle panel) or for acidified lysosomes (Figure 1D, upper-right panel). Addition of CI-976 caused a significant reduction in cellular LB content (Figure 1D, lower-left panel) with a concomitant increase in both autophagosomes and acidified lysosomes (Figure 1D, lower-middle and lower-right panels). We verified that the effects of CI-976 were indeed mediated through inhibition of ACATs by obtaining similar results after simultaneous silencing of *ACAT1* and *ACAT2* gene expression by small interfering RNA (siRNA; Figure S1).

Figure 1E depicts the inverse relationship between LB levels and that of autophagosomes and acidified lysosomes, whereas the CI-976 induced shift in steady state between the proportions of persisting bacteria in lipidic environment versus that present in degradative vesicles is shown in Figure 1F. Similar results were obtained when the experiments were performed in peripheral blood mononuclear cell (PBMC)-derived primary human macrophages (Figure S1), thus verifying the functional relevance of these findings. Further, as expected, the CI-976-mediated increase in H37Rv association with autophagosomes/lysosomes also correlated with a dose-dependent increase in bacterial killing (Figure 1G). Thus, inhibition of LB formation shifts the cellular homeostatic balance in favor of increased mycobacterial killing.

LB Formation in H37Rv-Infected Macrophages Correlates with an Increase in Levels of Nonphosphorylated Perilipin

LB formation is regulated by the cAMP-dependent signaling pathway, which modulates turnover rates of TAGs (Tansey et al., 2004). Stimuli that reduce intracellular cAMP levels diminish lipolysis rates and promote LB formation (Brasaemle, 2007). Consistent with this, addition of the adenylate cyclase inhibitor D7408 to uninfected cells caused enhanced LB accumulation (Figure S1), confirming the TAG-regulatory role for cAMP in THP-1 cells.

Infection of THP-1 cells with either H37Ra or H37Rv led to an initial burst of comparable magnitude in intracellular cAMP levels (Figure 2A). Agarwal et al. (2009) have shown that this increased cAMP is of mycobacterial origin, a product of the activity of the adenylate cyclase gene *Rv0386*. However, whereas the cAMP levels in H37Ra-infected cells were maintained at the elevated concentration, a subsequent time-dependent decrease to below baseline levels was observed in the case of H37Rv-infected cells (Figure 2A). Thus, in contrast to the situation with the avirulent strain H37Ra, the early cAMP burst initiated upon infection with H37Rv represented a transient phenomenon that was then succeeded by the active suppression of cAMP accumulation in the host cell.

To evaluate the consequences of this later phase of cAMP inhibition on TAG lipolysis we examined for effects on phosphorylation of perilipin, the central regulator of lipid storage. Nonphosphorylated perilipin coats lipid droplets and thereby protects them from lipase activity. PKA-dependent phosphorylation, however, induces a conformational change, as a result of which the stored lipids are rendered vulnerable to hormone-sensitive lipase (HSL) mediated lipolysis (Brasaemle 2007). While no detectable effect was seen with H37Ra, infection of THP-1 cells with H37Rv resulted in a significant increase in cellular perilipin levels (Figures 2B and 2C).

Interestingly, the buildup in perilipin concentrations was also accompanied by a marked reduction in the extent of phosphorylation (Figure 2B). The combined effects of H37Rv infection of inducing de novo synthesis of perilipin on the one hand, while simultaneously inhibiting its PKA-dependent phosphorylation on the other, caused a substantial decrease in the phoshoperilipin to perilipin ratio (Figure 2D). This shift in favor of nonphosphorylated perilipin then likely increases protection of TAGs against lipolysis, thereby promoting LB accumulation.

Mtb-Dependent LB Formation Is Mediated through the G Protein-Coupled Receptor GPR109A

To identify host proteins that regulated pathogen load, we had previously performed a genome-wide RNA interference (RNAi) screen against host factors in macrophages infected with H37Rv. The targets thus identified were then further filtered in a subscreen employing cells that were separately infected with a diverse panel of field isolates. This enabled definition of a core subset of host proteins that constituted dependency factors for at least a broad spectrum of genotypically and phenotypically distinct Mtb strains (Kumar et al., 2010). An inspection of this list revealed one of the members to be the Gi protein-coupled receptor GPR109A.

GPR109A belongs to the subfamily of hydroxycarboxylic acid receptors, all of which mediate antilipolytic effects in adipocytes (Ahmed et al., 2009). While it was originally characterized as the receptor for the antidyslipidemic drug nicotinic acid (NA) (Tunaru et al., 2003), recent studies have identified the ketone body D-3-hydroxybutyrate (3HB) as the endogenous ligand for this protein (Taggart et al., 2005). Activation of GPR109A couples it to the G_i-type G proteins causing an inhibition of adenylyl cyclase and the consequent reduction in cellular cAMP levels account for the antilipolytic effects of this receptor (Offermanns, 2006). Therefore, given the dependency of Mtb on this protein for intracellular sustenance, we speculated that GPR109A could be recruited by H37Rv to mediate FM differentiation.

Stimulation of THP-1 cells with either NA or 3HB caused a reduction in cellular cAMP levels, although the endogenous ligand 3HB was more effective (Figure 2E). Importantly, this effect was reversed in the presence of mepenzolate bromide (MPN), a specific inhibitor of GPR109A (Rask-Andersen et al., 2011). Further, addition of either NA or 3HB to cells also led to increased LB accumulation, but again in an MPN-sensitive manner (Figure 2F), confirming that the antilipolytic activity of GPR109A was also retained in macrophages.

Significantly, the H37Rv-mediated reduction in cAMP concentrations and the consequent accumulation of LBs in THP-1 cells could both be completely inhibited by the addition of MPN (Figures 2G and 2H). The GPR109A-dependent specificity of these effects was verified by experiments demonstrating that siRNA-mediated depletion of this protein also abrogated the ability of H37Rv to suppress cAMP production in THP-1 cells thereby mitigating LB formation (Figure S2). Thus, GPR109A activation represents at least the predominant mechanism by which mycobacterial bacilli induce LB formation in the host macrophage. Finally, similar to the findings with CI-976, MPN-dependent inhibition of LB formation was accompanied by a reversal of the block in autophagy, lysosome acidification, and the development of a respiratory burst (Figure S2).

H37Rv-Dependent Activation of GPR109A Involves a 3HB-Mediated Autocrine/Paracrine Loop

Related experiments revealed that the culture supernatant from H37Rv-infected but not from either uninfected or H37Ra-infected cells was alone sufficient to induce LB formation in THP-1 cells and this response was also inhibited by the presence of MPN (Figure 3A), implying that H37Rv-infected cells likely secreted an agonist for GPR109A. Therefore, we next sought

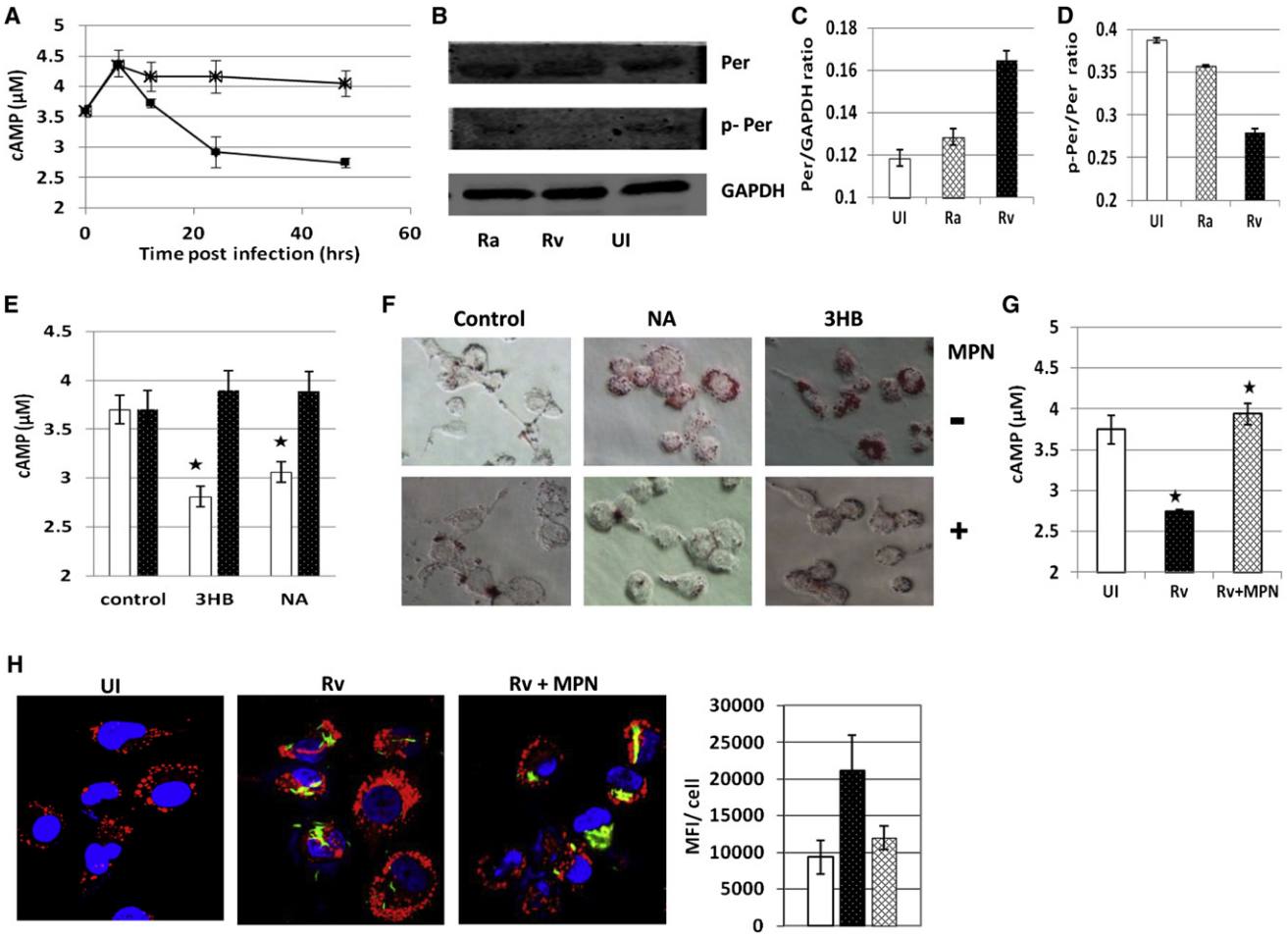

Figure 2. H37Rv-Directed LB Formation in Host Macrophages Is Mediated through GPR109A Activation

(A) Time-dependent effects of infection of THP-1 cells with either H37Ra (stars) or H37Rv (filled squares) on cellular cAMP levels (n = 3; mean ± SD).

(B–D) The corresponding effects on the levels of both perilipin (Per) and its phosphorylated subset (pPer) as determined by a western blot analysis at 48 hr p.i are shown (B). A quantitative representation of this is depicted in (C), whereas (D) illustrates the consequent effects on the ratio of the phosphorylated versus nonphosphorylated perilipin (n = 3; mean ± SD).

(E) Effect of addition of either 3HB or NA (10 μM) on cAMP levels in uninfected cells. Addition was performed either in the absence (open bars) or presence (100 nM, filled bars) of MPN (n = 3 ± SD; significance, *$p \leq 0.05$).

(F) LB-inducing effect of 3HB and NA (–), and its sensitivity to MPN addition (+). LBs were detected here by staining with oil red O, followed by visualization under a light microscope.

(G) The H37Rv-induced (filled bar) reduction in cAMP levels (open bars) is reversed upon MPN addition (hatched bars). MPN was added at 6, 16, and 40 hr p.i. The time point of measurement was 48 hr p.i. (n = 3 mean ± SD; significance, *$p \leq 0.05$).

(H) Confocal microscopy images comparing LBs (red) in uninfected cells and cells infected with GFP-tagged H37Rv (green) left untreated or treated with MPN as described for (G) are shown. DAPI (blue) was used for staining the nuclei. The extreme right panel provides a quantitative measure of LB levels, as MFI/cell, in uninfected cells (open bar), infected cells (filled bar), and in MPN-treated infected cells (hatched bar). Values are the means ± SE obtained from at least 50 cells. See also Figure S2.

to measure the levels of 3HB, the endogenous ligand for this receptor, in the culture supernatants.

Infection of THP-1 cells with H37Rv led to a clear time-dependent accumulation of 3HB in the culture supernatant. In contrast, only marginal levels of 3HB were detected at any of the time points studied in H37Ra-infected cells (Figure 3B). Thus, in comparison with its avirulent counterpart, H37Rv more vigorously induced 3HB synthesis and/or secretion from the host macrophage which can then be expected to activate GPR109A in an autocrine/paracrine fashion. We separately determined the EC_{50} of 3HB for GPR109A activation (in terms of cAMP inhibition) in THP-1 cells to range between 5 to 10 μM. The concentrations achieved by H37Rv-infected cells in Figure 3B are therefore sufficient to ensure early activation of GPR109A.

3HB Is Synthesized through a Nonclassical Pathway in H37Rv-Infected Cells

Ketone bodies are generally synthesized by hepatocytes in response to metabolic stress. Under conditions of either starvation or of uncontrolled diabetes, fatty acid (FA) metabolism switches from the direction of synthesis to that of oxidative degradation (McGarry and Foster, 1980). The acetyl-CoA thus

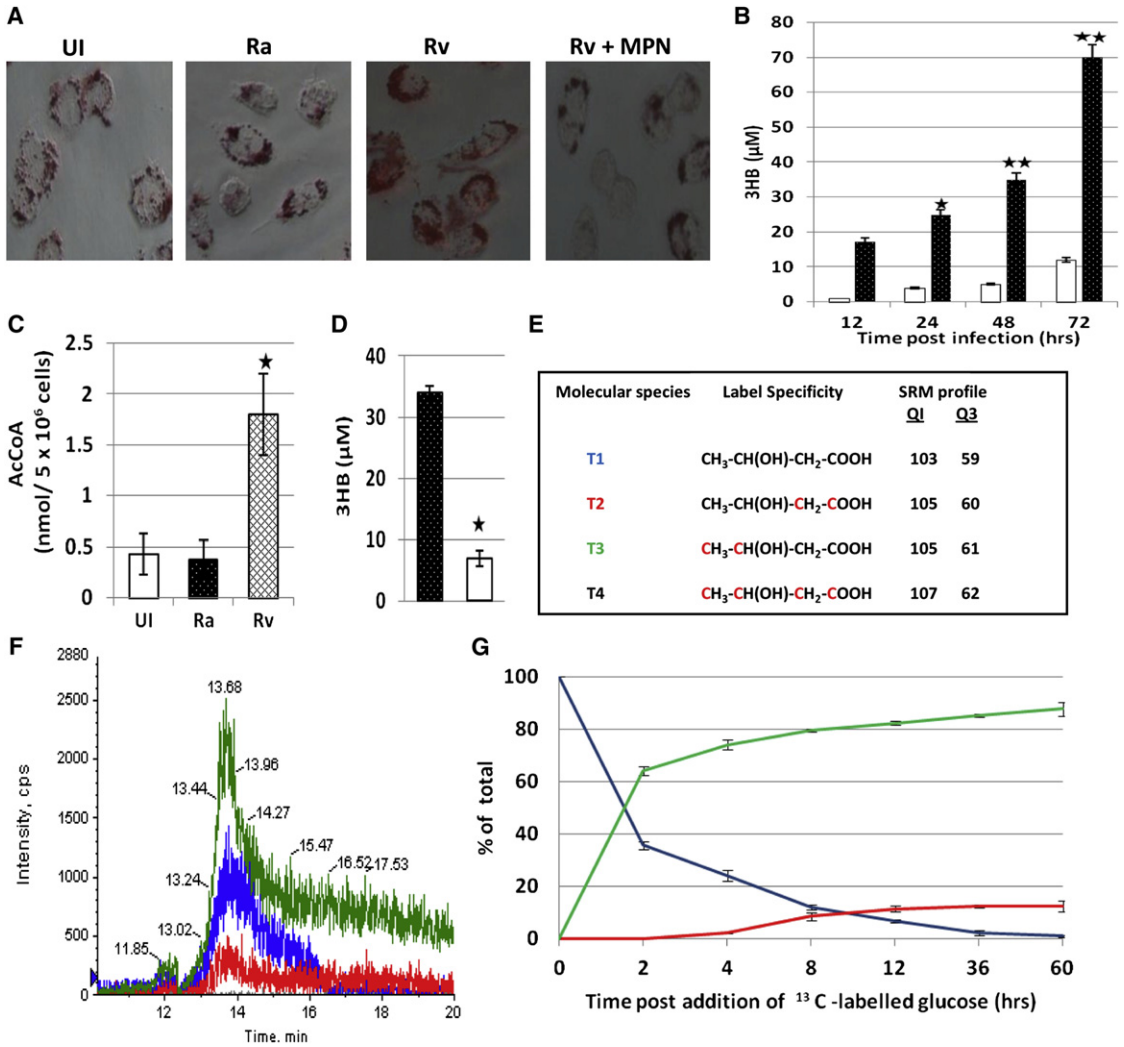

Figure 3. Mtb-Dependent Activation of GPR109A Is Mediated through Induction of 3HB Synthesis

(A) Culture supernatants from uninfected, H37Ra-infected, or H37Rv-infected THP-1 cells (at 48 hr p.i.) were collected and used to replace the medium of a fresh culture of uninfected THP-1 cells. Forty-eight hours later, these cells were stained with oil red O, and the extent of LB formation was monitored. The increased LB response after addition of supernatant from H37Rv-infected could be inhibited by the addition of MPN (Rv + MPN).

(B) Time-dependent accumulation of 3HB in culture supernatants of cells infected with either H37Ra (open bars) or H37Rv (filled bars) (n = 3, mean ± SD; significance, $^{**}p \leq 0.01$, $^{*}p \leq 0.05$).

(C) Host cellular concentrations of acetyl-CoA in uninfected (open bar), H37Ra-infected (filled bar), or H37Rv-infected (hatched bar) cells, as measured by mass spectrometry at 12 hr p.i. (n = 5, mean ± SD).

(D) The inhibitory effect of exogenous addition of palmitic acid (10 μM, open bar) on 3HB production by H37Rv-infected cells. Filled bar gives the 3HB concentration obtained in the absence of any addition (n = 3, mean ± SD; significance, $^{*}p \leq 0.05$).

(E) The expected individual molecular ion species for 3HB, and their SRM transitions, after addition of uniformly labeled ^{13}C-glucose to H37Rv-infected cells are shown.

(F) An extracted ion chromatogram, at 4 hr, displaying the relative distribution of 3HB between the T1 (blue), T2 (red), and T3 (green) molecular ions.

(G) Results of a time course analysis showing the accumulation of both T2 (red line) and T3 (green line) at the expense of the parent molecular species T1 (blue line) (n = 3, mean ± SD).

See also Figure S3.

produced is utilized to generate acetoacetate and 3HB via the reactions of the HMG-CoA cycle (Fukao et al., 2004). Therefore, it was conceivable that infection with H37Rv caused a perturbation of the metabolic state of the host cell, which then augmented FA catabolism to cause acetyl-CoA accumulation.

An indicator of the metabolic perturbation that favors ketone body formation is the ratio of acetyl-CoA versus oxaloacetate concentrations in the cell (Siess et al., 1982). This reflects the steady state between acetyl-CoA generation and its recruitment into the TCA cycle (Battersby et al., 1985). Host cell metabolites were extracted from H37Ra and H37Rv infected cells at 12h p.i. for determining the levels of acetyl-CoA and oxaloacetate by mass spectrometry. Relative to that in uninfected cells, H37Ra infection did not cause any significant perturbation in the levels

of acetyl-CoA (Figure 3C). Infection with H37Rv, however, induced a near 5-fold increase in this value (Figure 3C). In contrast to the differential effects on acetyl-CoA, oxaloacetate concentrations were unaffected and remained comparable in all three cases (0.85–1.0 nmole/5 × 10^6 cells). This finding that only H37Rv infection caused excess generation of acetyl-CoA therefore also rationalizes the selective ability of this Mtb strain to activate 3HB production by the host cell (Figure 3B).

Surprisingly, addition of etomoxir to H37Rv-infected cells had no detectable effect on 3HB production (data not shown). Etomoxir is an irreversible inhibitor of O-carnitine palmitoyltransferase and therefore prevents FA transport into the mitochondria for oxidative degradation (Xu et al., 2003). This indication that FA catabolism may not be responsible for 3HB production was also supported by findings that addition of uniformly labeled ^{13}C-palmitic acid to H37Rv-infected cells did not yield any ^{13}C-labeled 3HB, as determined by mass spectrometry (data not shown). On the contrary, addition of palmitic acid to infected cells led to a near 80% inhibition in the 3HB concentration of the resulting culture supernatant (Figure 3D). Importantly, this effect was not due to any toxic effects of FA on the intracellular bacilli (Figure S3).

Pyruvate, a product of glycolysis, may also alternately contribute to ketone body synthesis, at least in hepatocytes (Battersby et al., 1985). Figure 3D, showing that free FA inhibits H37Rv-induced 3HB production, supported the relevance of such a possibility to the present case. FAs are known to inactivate the pyruvate dehydrogenase complex, which is responsible for converting pyruvate into acetyl-CoA in the mitochondria (Wieland et al., 1972). Consistent with this, we found that treatment of H37Rv-infected THP-1 cells with palmitic acid led to a greater than 3-fold increase in steady-state concentrations of pyruvate, with a concomitant 6-fold decrease in acetyl-CoA levels (Figure S3).

To further confirm this implied involvement of the glycolytic pathway, we next cultured H37Rv-infected cells in the presence of uniformly labeled ^{13}C-glucose and examined for label incorporation in 3HB by mass spectrometry. Here, the presence of molecular species incorporating different sets of ^{13}C-carbon atoms was analyzed by single-reaction monitoring. We probed for all the four molecular ions that were theoretically possible. One was a 3HB molecular ion with no ^{13}C incorporation (T1), and the second was 3HB with the carbon atoms at positions 1 and 2 incorporating the label (T2). The third species represented label incorporation at carbon atoms at positions 3 and 4 (T3), whereas the fourth represented a 3HB molecule where all the four carbons were labeled (T4). These parent molecules, along with the expected masses for the parent and the resulting fragment ions, are shown in Figure 3E. A representative extracted ion chromatogram obtained in these experiments is shown in Figure 3F.

A time course analysis revealed that the ^{13}C-label was indeed incorporated into 3HB although surprisingly, only the T3 molecular ion was generated as the dominant species (Figure 3G). A rapid conversion of T1 into T3 was seen within the first 2 hr. Although the rate of this process slowed thereafter, levels of T3 nonetheless reached 90% of the total 3HB concentration by 60 hr, at which time T1-3HB was virtually undetectable (Figure 3G). The T2 species remained insignificant up to 4 hr, after which its concentration saturated at ~10% of total 3HB by 8 hr (Figure 3G). Significantly, the T4 molecular ion was not detected at any of the time points studied.

These results confirm that the glycolytic pathway at least partially contributes toward H37Rv-induced 3HB production by THP-1 cells. Notably, however, of the two acetyl-CoA units incorporated in 3HB, only one was derived from the glycolytic pathway. The source of the second unit is presently unknown and may derive either from the catabolism of ketogenic amino acids or from a separate acetyl-CoA pool with very slow turnover rates. The predominance of T3 (Figure 3G) also implies a compartmentalization of acetyl-CoA pools that are derived from glycolysis and the alternate mechanisms. The two possible pathways that can yield a directed synthesis of 3HB where the acetyl-CoA generated from glycolysis is selectively incorporated as the reduced unit in 3HB are shown in Figure S3.

The Ability to Induce 3HB Production from the Host Macrophage Correlates with Virulence Properties of the Infecting Mycobacterial Strain

To probe whether the potency of 3HB induction in macrophages was a feature that distinguished the virulence properties of mycobacteria, we next studied a larger panel of both attenuated and virulent strains. THP-1 cells (Figure 4A) or human PBMC-derived macrophages (Figure 4B) were individually infected with each of these and 3HB levels in the resulting culture supernatants were measured. In both instances, infection with virulent Mtb strains led to secretion of significant levels of 3HB, whereas only marginal concentrations of this compound were detected when cells were infected with any of the attenuated strains (Figures 4A and 4B). Consistent with this result, LB accumulation was also observed only in cells infected with the virulent strains (Figure S4). Thus, at least in the context of the panel tested here, the ability to activate 3HB synthesis and consequent FM differentiation appears to constitute a trait that distinguishes virulent from the attenuated strains.

The distinction observed between the virulent and avirulent strains could merely reflect the fact that whereas the former grow and persist in the macrophages, the latter do not. We therefore profiled the time-dependent changes in infection load for these strains both in THP-1 cells and in primary human macrophages. The avirulent strains yielded the expected profile of a steady decline in intracellular bacillary load with time (Figures 4C and 4D). In contrast, the majority of the virulent strains tested displayed a time-dependent increase in bacterial counts, albeit with different kinetics. A notable exception here, however, was JAL2261. The overall growth profile of this strain in both THP-1 cells and primary human macrophages was comparable to that obtained for the avirulent Mtb strains (Figures 4C and 4D). However, Figures 4A and 4B show that the poor growth capacity of JAL2261 in macrophages did not compromise its ability to activate 3HB production from the host cell. This finding therefore argues against a direct relationship between the 3HB-induction capacity of a Mtb strain and its growth properties in macrophages. Rather, the former likely derived from some other molecular feature that characterized mycobacterial virulence.

Although ketomycolic acids have been suggested to play a role in the Mtb-induced FM differentiation (Peyron et al., 2008), a mass spectrometric analysis of lipids extracted from

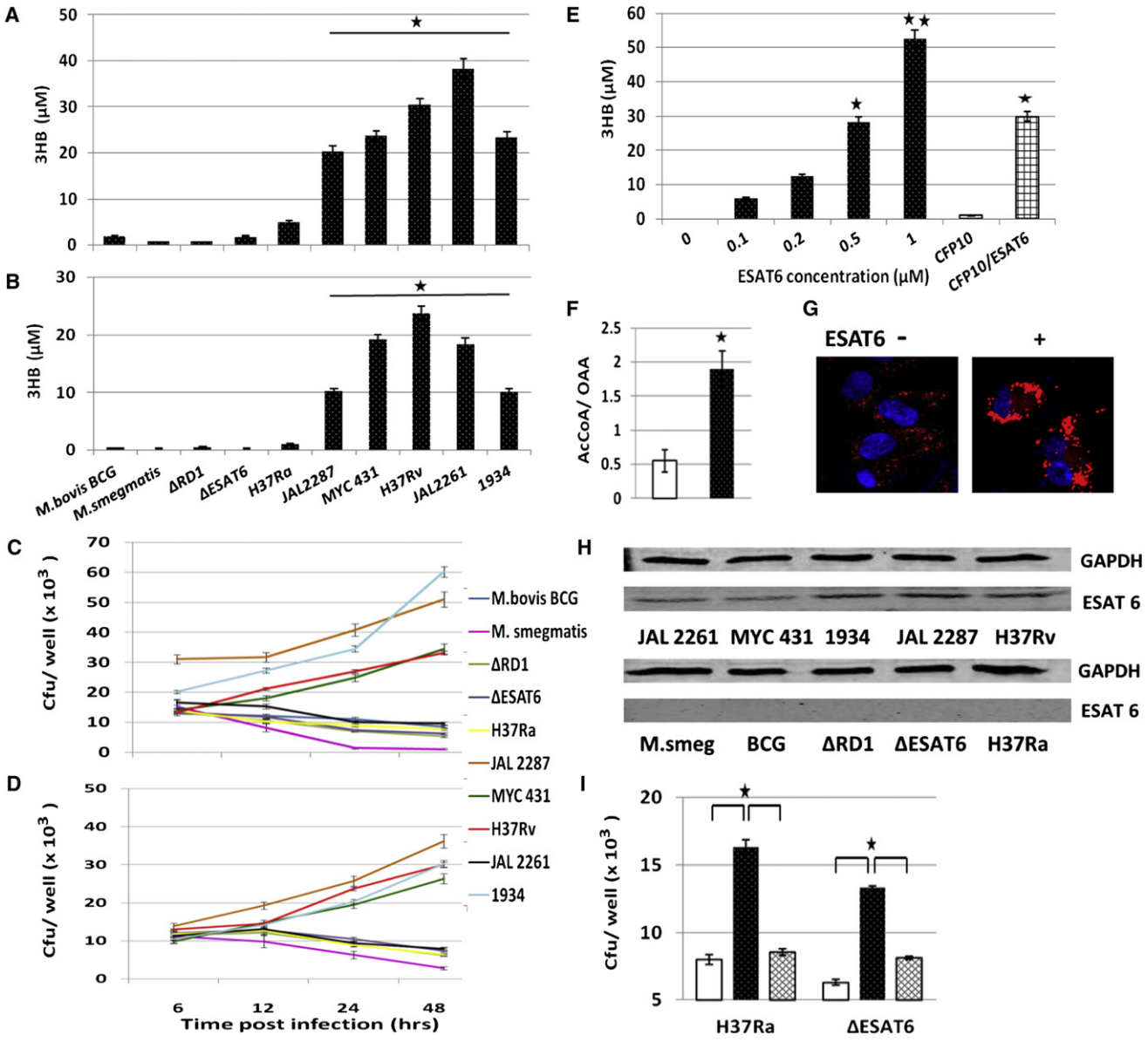

Figure 4. Only Pathogenic Mtb Strains Induce 3HB Production from the Host Macrophage

(A) THP-1 cells were infected with a panel of attenuated (*M. bovis* BCG, *M. smegmatis*, *M. tuberculosis* H37Ra, ΔRD1, and ΔESAT6) and virulent strains of Mtb (*M. tuberculosis* H37Rv, 1934, JAL2287, JAL2261, and MYC431). The levels of 3HB in the culture supernatants were subsequently measured at 48 hr p.i.

(B) A similar experiment was also performed in primary human PBMC-derived macrophages (n = 3, mean ± SD; significance, *p ≤ 0.05).

(C and D) The growth profiles of these strains in THP-1 cells (C) and primary human macrophages (D) (n = 3, mean ± SD).

(E) Effect of exogenous addition of increasing concentration of ESAT-6 protein, CFP-10 (1 μM), and complex of ESAT-6 and CFP-10 (final concentration of 0.5 μM) on 3HB production by uninfected THP-1 cells, measured at 48 hr (n = 3, mean ± SD; significance, **p ≤ 0.01, *p ≤ 0.05).

(F) Ratio of acetyl-CoA versus oxaloacetate either in unstimulated THP-1 cells (open bar) or in cells stimulated with ESAT-6 (0.5 μM) for 6 hr (filled bar) (n = 3, mean ± SD).

(G) LB content in THP-1 cells that had been either left untreated (–) or treated (+) with ESAT-6 for 48 hr.

(H) Western blot analysis for the presence of ESAT-6 in lysates of THP-1 cells infected with the individual Mtb strains, generated at 48 hr p.i. GAPDH was used as the loading control.

(I) THP-1 cells infected with H37Ra or with the ΔESAT-6 strain were left untreated (open bars) or treated wither either ESAT-6 (filled bars) or a combination of ESAT-6 and MPN (hatched bar). The cfu was determined at 48 hr p.i., and data are from one of two experiments (mean ± SE of triplicate wells).

See also Figure S4 and Table S1.

the strains in Figure 4A did not identify any distinguishing feature between the virulent and avirulent strains (Figure S4). Rather, our results in Figures 4A and 4B revealing that deletion of the *esat-6* gene from H37Rv caused a loss in ability to induce 3HB from infected macrophages supported a likely role for the ESAT-6 protein. We verified this possibility by demonstrating that

complementation of the deletion mutant with a plasmid bearing the intact *esat-6* gene restored its capacity to generate 3HB from infected THP-1 cells (Figure S5). Further substantiation was then obtained by experiments demonstrating that addition of the ESAT-6 protein alone to uninfected THP-1 cells induced a dose-dependent increase in 3HB production (Figure 4E). Its counterpart CFP-10 did not share this property, although the ESAT-6-resident activity was also retained in the heterodimeric complex of CFP-10 and ESAT-6 (Figure 4E). More importantly, the ESAT-6-induced predilection for ketone body synthesis was reflected at the level of an increased acetyl-CoA to oxaloacetate ratio in the macrophages (Figure 4F), and this process then culminated in the induction of FM differentiation (Figure 4G). Separate experiments involving ^{13}C-glucose labeling also confirmed that the pattern of ^{13}C-label incorporation into 3HB was identical to that described in Figure 3F (Figure S5), thus indicating that the ESAT-6-activated pathway was at least similar to that seen in H37Rv-infected cells.

Our above findings thus rationalize the inability of the attenuated strains to activate 3HB production from the host macrophage (Figures 4A and 4B). *M. bovis* BCG, H37Ra, and the ΔESAT6 and ΔRD1 mutants of H37Rv are all incapable of secreting ESAT-6 (Mahairas et al., 1996; Frigui et al., 2008; Lewis et al., 2003). The ESAT-6 protein of *M. smegmatis*, on the other hand, differs both in sequence and properties from that of its Mtb analog (Gey van Pittius et al., 2002). As expected, therefore, the presence of ESAT-6 could clearly be detected in lysates of THP-1 cells that had been infected with the virulent, but not the attenuated mycobacterial strains (Figure 4H). Further, at least some of this protein was also secreted into the culture supernatant (Figure S4).

Addition of ESAT-6 protein to THP-1 cells that had been infected either with the ΔESAT6 strain or with H37Ra led to the expected increase in LB formation (Figure S5). More importantly though, this also substantially improved the intracellular viability of both strains, and this effect was sensitive to the presence of MPN (Figure 4I). Collectively, therefore, the results in Figures 4E-I confirm at least a prominent role for ESAT-6 in activating 3HB production from the host cell, thereby causing them to differentiate into FMs.

GPR109A Is an Effective Target for Anti-TB Drug Development

The exploitation of the LB-induction pathway by all virulent Mtb strains tested suggested that GPR109A inhibition could serve as an efficient way to reduce the bacillary burden in infected macrophages. To test this, we took H37Rv and four of the field isolates described in Figure 4A. JAL2287, JAL2261, and 1934 were MDR-Mtb strains but with distinct drug-resistance profiles (Table S1). Further, the clade origins of JAL2261 and 1934 (Manu) also differed from that of JAL2287 (CAS). MYC431 was an extremely drug-resistant isolate of Mtb (XDR-Mtb) that belonged to the Beijing superfamily (Table S1). THP-1 cells were separately infected with each of these strains and then treated with varying doses of MPN. Figure 5A demonstrates that MPN treatment significantly compromised, in a dose-dependent manner, survival of all of the strains tested with comparable EC_{50} values (2–6 nM). The efficacy of MPN against these strains was also retained in the context of infection of primary human macrophages (Figure 5B). Importantly, in both instances, viability of the host cell was unaffected by MPN treatment. Further, MPN also had no detectable effect on extracellular cultures of the individual Mtb strains at the level of viability, cell wall integrity, or lipid composition (Figure S5 and Table S2).

We also employed transmission electron microscopy (TEM) to visualize the effects of MPN on intracellular bacilli. THP-1 cells were infected with one of three representative strains (H37Rv, JAL2287, or MYC431) from the panel studied in Figure 5A. Sections generated from MPN-treated and untreated cells at 60 hr p.i. were scored for the proportion of individual cell slices that showed the presence of bacteria. A marked reduction in the frequency of infected cells, after MPN treatment, was observed in all cases (Figure 5C). In addition, the intracellular bacillary load was also substantially reduced in those few residual cells where the infection persisted after MPN treatment (Figures 5D and 5E). These results further corroborate the bactericidal consequences of MPN-dependent inhibition of GPR109A activation.

We next evaluated the efficacy of MPN in the murine model of TB infection. Since our intent was primarily to demonstrate "proof of concept," we employed only a short-term treatment regimen in these experiments. BALB/c mice infected through the aerosol route either with H37Rv, JAL2287, or MYC431 were treated with a dose of 2 mg/kg body weight of MPN. Subsequently, the mice were sacrificed and bacterial loads in the lungs, liver, and spleen were determined.

MPN treatment caused a clear and significant decline in the level of infection in all the three organs examined and was comparable for the three Mtb strains tested (Figure 6A). Histochemical staining of lung sections reiterated that the numbers of acid-fast staining bacilli were indeed reduced (Figure 6B), with a concomitant attenuation of the granuloma response in terms of both the numbers of granulomas detected and the reduced size of those that persisted (Figures 6C and 6D). Further, the LB content was also diminished in alveolar macrophages of MPN-treated mice (Figure S6). Finally, at a more gross level recovery from infection-induced splenomegaly was also evident (Figure 6E).

The results in Figures 5 and 6 thus highlight the potential of GPR109A as target for the development of anti-TB drugs. Pertinent here is our demonstration of the comparable efficacy of this approach against infections with drug-sensitive (H37Rv), multiple drug-resistant and extremely drug-resistant strains of the pathogen-independent of their clade identity.

DISCUSSION

Alveolar FMs play a prominent role in guiding the granuloma response to Mtb infection (Hunter et al., 2007, Russell et al., 2009, 2010). In nonnecrotizing granulomas, infection is primarily restricted to FMs wherein mycobacteria are predominantly engulfed within LBs (Peyron et al., 2008). This LB encapsulation provides a privileged existence for the encapsulated bacilli through the ready provision of nutrients on the one hand (Peyron et al., 2008) and by conferring protection against inflammatory and other bactericidal pathways on the other (Peyron et al., 2008; D'Avila et al., 2006). Further, bacilli within LBs switch into a dormant nonreplicative state, thereby also increasing

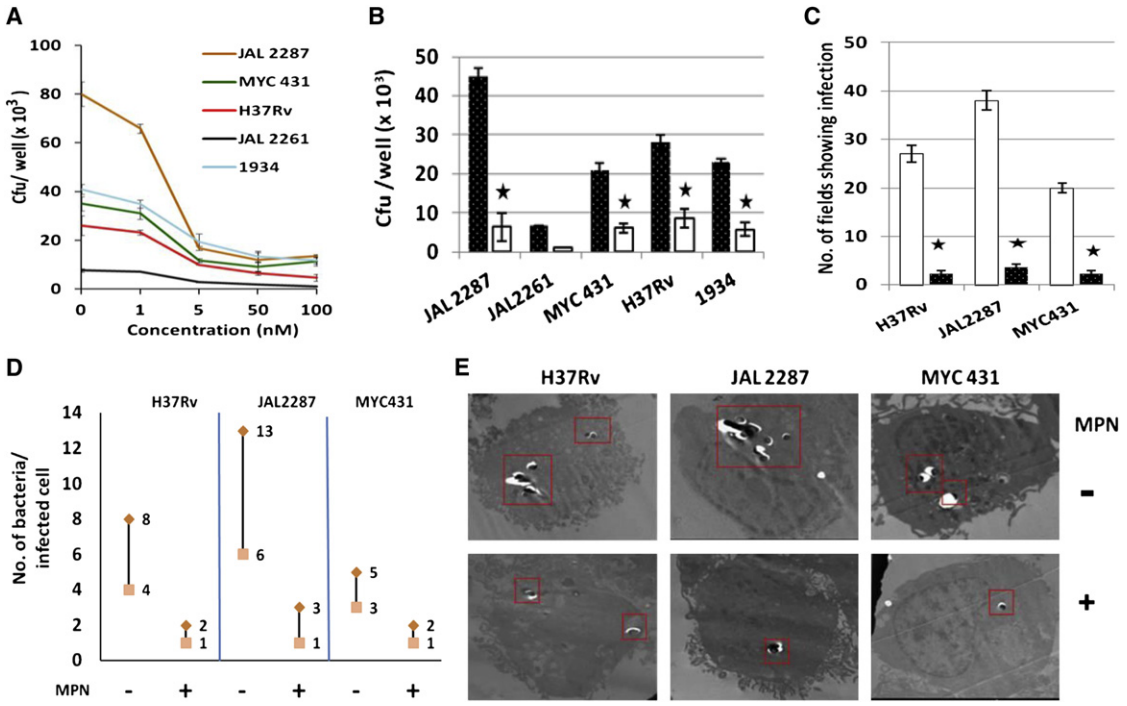

Figure 5. Targeted Inhibition of GPR109A Reduces Intracellular Bacillary Load

(A) Dose-dependent effects of MPN on mycobacterial cfu in THP-1 cells infected with the indicated virulent Mtb strains.

(B) Results of a similar experiment performed in primary human PBMC-derived macrophages except that a single dose (100 nM) of MPN was used. For both experiments values are mean ± SD of at least three determinations.

(C) THP-1 cells infected with H37Rv, JAL2287, or MYC431 were left untreated or treated with MPN (100 nM). The cells were harvested at 60 hr p.i. and processed for transmission electron microscopy (TEM). Sections were scored for the proportion of cell slices that showed the presence of one or more bacteria. A total of 50 cell sections were enumerated and the number of those displaying the presence of Mtb in both untreated (open bars) and MPN-treated (filled bars) is shown (n = 3, mean ± SD; significance, *$p \leq 0.05$).

(D) The range of bacterial numbers obtained per infected cell in the sections counted in (C) is shown.

(E) The reduction in the number of bacteria on a per-cell basis is illustrated by the representative TEM images. Here the bacilli are identified within the red boxes. See also Figure S5 and Table S2.

their threshold of drug-sensitivity (Peyron et al., 2008; Daniel et al., 2011).

Our study reveals yet another level at which FMs contribute toward safeguarding the intracellular Mtb. As shown, accumulation of LBs correlated with an inhibition of both autophagy and lysosome acidification. While the mechanistic basis of this reciprocal crosstalk is presently unknown, it may relate to the primary function of autophagy as a cellular sensor of nutrient deprivation. Independent of the specifics though, the overall importance of FMs to Mtb survival could be confirmed by experiments demonstrating a profound reduction in bacillary load, under conditions where LB biogenesis was inhibited. Conversely, forced induction of LB formation in the host cell also led to improved intracellular survival of attenuated mycobacteria. Thus, our understanding of the role that FMs play in the disease process has significantly advanced over the years. In contrast, though, we remain ignorant about the mechanisms that Mtb co-opts to induce differentiation of these cells. It is in this context that our present study assumes significance, as it provides insights toward this direction.

We discovered that Mtb-induced FM differentiation was mediated through activation of a feedback loop involving the host cell-specific antilipolytic GiPCR, GPR109A. Activation of this receptor induced a reduction in the level of cellular cAMP, which then caused a decrease in the extent of perilipin phosphorylation. The resultant predominance of nonphosphorylated perilipin over its phosphorylated form likely then protected the TAGs against lipase action, thereby leading to LB accumulation.

Especially relevant was our delineation of the mechanism employed by the pathogen, in order to recruit the GPR109A-dependent feedback loop. Our results suggest that intracellular mycobacteria perturbed the flux between glycolysis and the TCA cycle in the host cell, leading to excess accumulation of acetyl-CoA. At least some of this excess acetyl-CoA was then shunted toward the synthesis of 3HB, the natural ligand for GPR109A. Secretion of this ketone body subsequently induced autocrine/paracrine activation of GPR109A, and the observed reduction in cellular cAMP levels was a direct product of this activation. Our finding that activation of 3HB production by infected macrophages was specific to virulent, but not attenuated, strains of Mtb could at least partially be rationalized by results implicating a direct role in this process for ESAT-6, a secretory virulence factor that is encoded within the RD-1

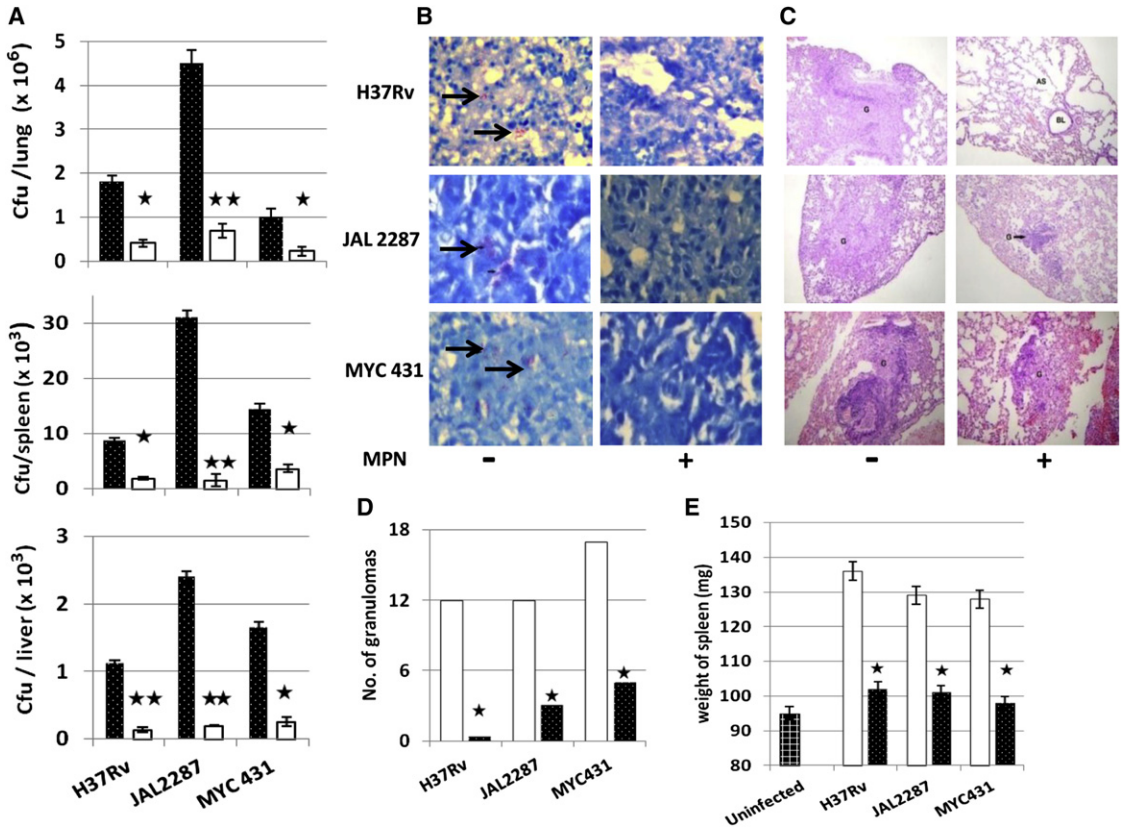

Figure 6. In Vivo Efficacy of MPN in the Murine Model of Mtb Infection

(A) Colony-forming units determined in lysates of lung, spleen, and liver from infected mice that were treated with vehicle only/control (filled bars) or MPN treated (open bars) are shown as mean ± SD. Data are representative of three separate experiments (significance, $^{**}p \leq 0.01$, $^{*}p \leq 0.05$).

(B) A comparison of lung sections of control (–) and MPN-treated (+) mice after staining with ZN indicates significant numbers of acid-fast bacilli in sections from control mice (indicated by arrows), which are absent in MPN-treated mice in all cases.

(C) Hematoxylin and eosin-stained lung sections show multiple well-formed granulomas with a mantle of lymphocytes in control mice (–). In contrast, these were absent in sections from H37Rv-infected mice treated with MPN, as well as substantially reduced in both numbers and size in mice infected with the remaining two strains, after MPN treatment (+).

(D) The total number of granulomas seen in three lung sections from infected mice that were treated either with the vehicle only (open bars) or with MPN (filled bars) are shown (significance, $^{*}p \leq 0.05$).

(E) Weights of the spleens from uninfected (hatched bar), control (open bars), and MPN-treated (filled bars) mice are compared. Values are the mean ± SD weight of spleens from five mice (significance, $^{*}p \leq 0.05$).

See also Figure S6.

gene locus of Mtb (Sørensen et al., 1995). While the mechanism by which this protein acts in the present context is under investigation, our initial results indicate that glucose uptake by macrophages is enhanced in its presence (Figure S6).

Evidence presented supports that the 3HB produced by Mtb-infected macrophages is of host rather than of mycobacterial origin. First, the effects of infection on acetyl-CoA accumulation and 3HB generation could be recapitulated simply by the addition of the ESAT-6 protein to uninfected macrophages. Further, in the presence of ^{13}C-glucose, the ^{13}C-labeling pattern of 3HB was identical in both cases. More conclusively, though, we found that RNAi-mediated silencing of expression of the human *mat* gene also abrogated 3HB production from H37Rv-infected THP-1 cells (Figure S6). The *mat* gene codes for the mitochondrial enzyme acetyl-CoA acetyltransferase, which converts acetyl-CoA into the 3HB intermediate, acetoacetyl-CoA. Thus, generation of 3HB, leading to GPR109A-dependent differentiation of FMs, is likely a direct consequence of mycobacterial manipulation of the host cellular metabolic pathways. A schematic of the feedback mechanism deduced from the present study is illustrated in Figure 7.

While we identify ESAT-6 as a critical mediator of FM differentiation, it is possible that this protein may also act cooperatively with other Mtb-derived molecular components such as oxygenated mycolic acids (Peyron et al., 2008), trehalose dimycolates (Bowdish et al., 2009), or other secreted proteins. Further the mechanism by which ESAT-6 perturbs the host cell metabolic flux to induce 3HB synthesis also remains to be clarified, although our preliminary results suggest that this may be mediated through the attenuation of TLR-2 signaling (Pathak et al., 2007). Thus, ESAT-6-dependent 3HB production by THP-1 cells was further augmented in the presence of the

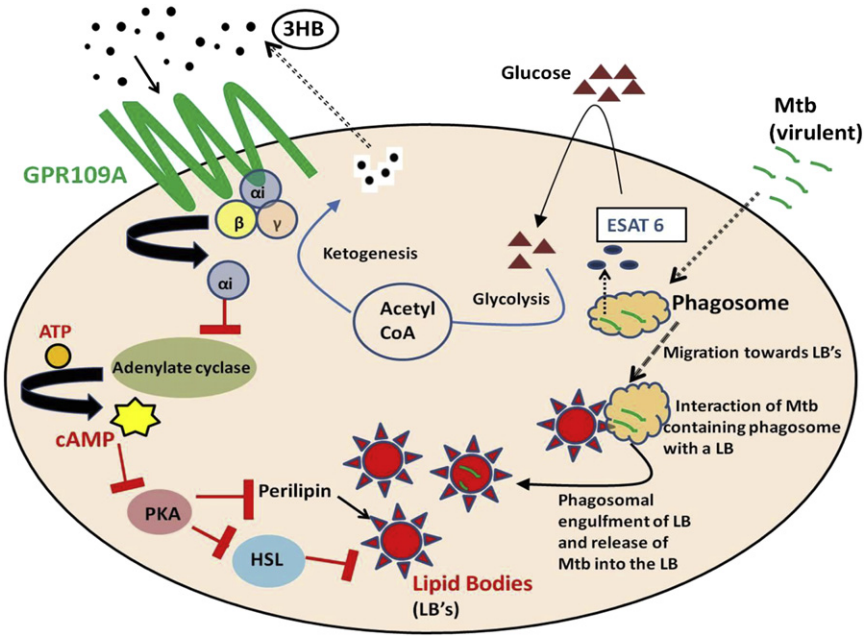

Figure 7. A Schematic of the Inferred Mechanism by which Virulent Mtb Strains Induce FM Differentiation

Upon entry into the host macrophage, Mtb secretes the ESAT6 protein, which then stimulates glucose uptake by the infected cell. This likely enhances the rate of glycolysis, leading to a net accumulation of acetyl-CoA. The excess acetyl-CoA is then partitioned toward the subsequent generation of 3HB through the HMG CoA cycle. Secreted 3HB activates GPR109A, causing inhibition of adenylyl cyclase activity. The consequent reduction in cellular cAMP levels attenuates activity of PKA as a result of which the extent of phosphorylation of perilipin is also reduced. Non-phosphorylated perilipin forms a protective coating at the LB surface and protects against lipolysis by HSL. This reduction in TAG turnover causes enhanced LB accumulation in the macrophage. Mtb containing phagosomes migrate toward these LBs, and eventually engulf them (Peyron et al., 2008). Subsequent release of the mycobacteria into these LBs then ensures protection from host cellular microbicidal pathways and thereby enables stable persistence of the bacilli.

TLR-2 antagonist OxPAPC, or in cells where *tlr2* gene expression was silenced by siRNA (Figure S6).

In keeping with the adopted function of FMs as secure havens for intracellular mycobacteria, selective inhibition of the Mtb-activated 3HB/GPR109A feedback loop with MPN resulted in a marked reduction in bacillary load. This effect was primarily due to a reduction in the magnitude of the LB response, because of which the antibacterial activities of the host cell were restored, leading to effective neutralization of mycobacterial virulence. Our experiments in infected mice further corroborated the benefits of exploiting GPR109A as a target for anti-TB drug development. Interestingly, this latter result supports the earlier speculation by Russell et al. (2010) that targeting the host lipid metabolic pathways that are perturbed by the mycobacteria may provide an indirect means to modulate disease progression.

The comparable potency displayed by MPN against infections with drug-sensitive and highly drug-resistant strains derived from different clades, particularly highlights the potential of this approach, given the near epidemic scenario that is now emerging in endemic regions due to the rapid spread of drug-resistant TB. While the abbreviated dosage regimen employed was sufficient to demonstrate "proof of concept," further developments will require an optimization of the protocol, as well as the generation of MPN analogs with better ADME properties. In addition, evaluation in animal models where the granuloma response more closely resembles the situation in humans also seems warranted. Such refinements should eventually pave the way for strategies that target the FM differentiation process as a means to at least control disease progression.

In summary, our present study provides insights into the mechanisms by which Mtb induces FM formation in macrophages. Importantly, it further identifies this step to serve as a filter for mycobacterial virulence and, therefore, function as an important determinant of disease outcome. Finally, also pertinent is our demonstration of how such information can be rationally exploited to develop TB chemotherapy.

EXPERIMENTAL PROCEDURES

Cell Culture, Infection, and cfu Determination

PMA-differentiated THP-1 cells were infected with mycobacteria at a multiplicity of infection of 10 during 4 hr of infection followed by amikacin treatment for 2 hr to remove any remaining extracellular bacteria as previously described (Kumar et al., 2010). Human PBMC-derived monocytes were isolated from heparinized blood by centrifugation on Ficoll-Paque and selection by adherence. The monocytes were allowed to spontaneously differentiate into macrophages. For cfu determination, infected cells were lysed in 0.06% SDS and plated on 7H11 agar plates supplemented with OADC and 0.5% glycerol.

Quantification of TAGs, cAMP, and 3HB

TAGs were measured after solubilizing cells in 5% (v/v) Triton X-100 with the Triglyceride Quantification Kit (Abcam). The cAMP Direct Immunoassay Kit (Abcam) was used to quantify cAMP levels in cell lysates. Culture supernatants were collected and the 3HB concentrations determined with the beta-HB Assay Kit (Abcam). For experiments involving incorporation of ^{13}C-label in 3HB, culture supernatants collected at the appropriate times were lyophilized and then extracted in methanol. The methanol extracts were dried and, after solubilizing in an aqueous solution of 10 mM tributylamine (pH 4.5), analyzed by liquid chromatography electrospray ionization tandem mass spectrometry (LC-ESI-MS/MS) on an Applied Biosystems/MDS Sciex Q 4000 TRAP linear ion trap mass spectrometer. Chromatographic separation was achieved on a C-18 column (Agilent) and the MS was operated in the negative ion and SRM mode.

Western Blot Analysis

Cell lysates were generated at 48 hr p.i. by solubilizing in a 20 mM HEPES buffer containing 0.5% Triton X-100 and supplemented with protease and/or phosphatase inhibitors as required. Cell extracts containing 50 μg protein was resolved on a SDS-polyacrylamide gel for subsequent western blot analysis. Perilipin rabbit mAb (CST), phospho-perilipin Ser522 mouse mAb (Vala Sciences), GAPDH rabbit mAb (Santa Cruz), and ESAT6 antibody HYB 076-08 (Abcam) were used for probing, and the blots were scanned with the Odyssey image scanner (Li-Cor).

Confocal Microscopy

Cells were stained with Lysotracker Red DND-99 (for acidified lysozomes), anti-LC3-II (for autophagosomes), LipidTox Red neutral lipid stain (for LBs), or DAPI (nucleus) as required. Stained cells were observed with a Nikon Eclipse Ti-E laser scanning confocal microscope equipped with 60×/1.4 NA PlanApochromat DIC objective lens. GFP, DAPI/LC3B, and Lysotracker/Lipid Tox were excited at 488 nm, 408 nm, and 543 nm with an argon ion, blue diode, and a Helium-Neon laser, respectively. The emissions were recorded through emission filters set at 515/30, 450, and 605/75. Serial confocal sections (0.5 μm thick) within a z stack spanning a total thickness of 10 μm were taken in individual channels green, blue, and red with the motor drive focusing system. Images were acquired with a scanning mode format of 512 × 512 pixels and analyzed with Image-Pro Plus version 6.0.

Animal Experiments

All animal experiments were carried out in accordance with guidelines approved and created by the ICGEB animal ethics committee. Female BALB/c mice, 4–6 weeks of age (five per group) were infected with H37Rv/JAL2287/MYC431 *M. tuberculosis* through aerosol exposure. MPN treatment at 2 mg/kg body weight was initiated at 15 days after infection in one group, while the control group was treated with the vehicle only. After two weeks of treatment, mice were sacrificed and mycobacterial load in lung, liver, and spleen was determined.

Statistical Analysis

Statistical significance was determined with the unpaired two-tailed Student's t test with Origin software. $p \leq 0.05$ was considered statistically significant.

SUPPLEMENTAL INFORMATION

Supplemental Information includes Supplemental Experimental Procedures, six figures, and two tables and can be found with this article online at http://dx.doi.org/10.1016/j.chom.2012.09.012.

ACKNOWLEDGMENTS

This work was supported by a DBT grant to K.V.S.R. V.S. is the recipient of a SRF from CSIR. V.S., S.J., R.J., and P.V. conducted the research. R.G. participated in the data interpretation and lipid analysis. V.S. and K.V.S.R. designed the research and wrote the manuscript. K.V.S.R. supervised the project. The authors acknowledge A. Kumar and Z. Siddiqui for assistance with the mycobacterial cultures, S. Kumar for help with the mice experiments, N. Saquib for the mass spectrometric analysis, and A. Basu (NIV) for help with the electron microscopy. MPN was a gift from Sphaera Pharma. All animal experiments were conducted in the DBT-funded TACF facility at ICGEB.

Received: April 3, 2012
Revised: June 27, 2012
Accepted: September 17, 2012
Published: November 14, 2012

REFERENCES

Agarwal, N., Lamichhane, G., Gupta, R., Nolan, S., and Bishai, W.R. (2009). Cyclic AMP intoxication of macrophages by a Mycobacterium tuberculosis adenylate cyclase. Nature *460*, 98–102.

Ahmed, K., Tunaru, S., and Offermanns, S. (2009). GPR109A, GPR109B and GPR81, a family of hydroxy-carboxylic acid receptors. Trends Pharmacol. Sci. *30*, 557–562.

Battersby, C.M., Alberti, K.G., and Agius, L. (1985). Conversion of pyruvate into ketone bodies in rat hepatocyte suspensions. Biochem. J. *231*, 565–569.

Bowdish, D.M., Sakamoto, K., Kim, M.J., Kroos, M., Mukhopadhyay, S., Leifer, C.A., Tryggvason, K., Gordon, S., and Russell, D.G. (2009). MARCO, TLR2, and CD14 are required for macrophage cytokine responses to mycobacterial trehalose dimycolate and Mycobacterium tuberculosis. PLoS Pathog. *5*, e1000474.

Brasaemle, D.L. (2007). Thematic review series: adipocyte biology. The perilipin family of structural lipid droplet proteins: stabilization of lipid droplets and control of lipolysis. J. Lipid Res. *48*, 2547–2559.

D'Avila, H., Melo, R.C., Parreira, G.G., Werneck-Barroso, E., Castro-Faria-Neto, H.C., and Bozza, P.T. (2006). Mycobacterium bovis bacillus Calmette-Guérin induces TLR2-mediated formation of lipid bodies: intracellular domains for eicosanoid synthesis in vivo. J. Immunol. *176*, 3087–3097.

Daniel, J., Maamar, H., Deb, C., Sirakova, T.D., and Kolattukudy, P.E. (2011). Mycobacterium tuberculosis uses host triacylglycerol to accumulate lipid droplets and acquires a dormancy-like phenotype in lipid-loaded macrophages. PLoS Pathog. *7*, e1002093.

Frigui, W., Bottai, D., Majlessi, L., Monot, M., Josselin, E., Brodin, P., Garnier, T., Gicquel, B., Martin, C., Leclerc, C., et al. (2008). Control of M. tuberculosis ESAT-6 secretion and specific T cell recognition by PhoP. PLoS Pathog. *4*, e33.

Fukao, T., Lopaschuk, G.D., and Mitchell, G.A. (2004). Pathways and control of ketone body metabolism: on the fringe of lipid biochemistry. Prostaglandins Leukot. Essent. Fatty Acids *70*, 243–251.

Gey van Pittius, N.C., Warren, R.M., and van Helden, P.D. (2002). ESAT-6 and CFP-10: what is the diagnosis? Infect. Immun. *70*, 6509–6510, author reply 6511.

Hunter, R.L., Jagannath, C., and Actor, J.K. (2007). Pathology of postprimary tuberculosis in humans and mice: contradiction of long-held beliefs. Tuberculosis (Edinb.) *87*, 267–278.

Krause, B.R., Anderson, M., Bisgaier, C.L., Bocan, T., Bousley, R., DeHart, P., Essenburg, A., Hamelehle, K., Homan, R., Kieft, K., et al. (1993). In vivo evidence that the lipid-regulating activity of the ACAT inhibitor CI-976 in rats is due to inhibition of both intestinal and liver ACAT. J. Lipid Res. *34*, 279–294.

Kumar, D., Nath, L., Kamal, M.A., Varshney, A., Jain, A., Singh, S., and Rao, K.V. (2010). Genome-wide analysis of the host intracellular network that regulates survival of Mycobacterium tuberculosis. Cell *140*, 731–743.

Lewis, K.N., Liao, R., Guinn, K.M., Hickey, M.J., Smith, S., Behr, M.A., and Sherman, D.R. (2003). Deletion of RD1 from Mycobacterium tuberculosis mimics bacille Calmette-Guérin attenuation. J. Infect. Dis. *187*, 117–123.

Mahairas, G.G., Sabo, P.J., Hickey, M.J., Singh, D.C., and Stover, C.K. (1996). Molecular analysis of genetic differences between Mycobacterium bovis BCG and virulent M. bovis. J. Bacteriol. *178*, 1274–1282.

McGarry, J.D., and Foster, D.W. (1980). Regulation of hepatic fatty acid oxidation and ketone body production. Annu. Rev. Biochem. *49*, 395–420.

Offermanns, S. (2006). The nicotinic acid receptor GPR109A (HM74A or PUMA-G) as a new therapeutic target. Trends Pharmacol. Sci. *27*, 384–390.

Pathak, S.K., Basu, S., Basu, K.K., Banerjee, A., Pathak, S., Bhattacharyya, A., Kaisho, T., Kundu, M., and Basu, J. (2007). Direct extracellular interaction between the early secreted antigen ESAT-6 of Mycobacterium tuberculosis and TLR2 inhibits TLR signaling in macrophages. Nat. Immunol. *8*, 610–618.

Peyron, P., Vaubourgeix, J., Poquet, Y., Levillain, F., Botanch, C., Bardou, F., Daffé, M., Emile, J.F., Marchou, B., Cardona, P.J., et al. (2008). Foamy macrophages from tuberculous patients' granulomas constitute a nutrient-rich reservoir for M. tuberculosis persistence. PLoS Pathog. *4*, e1000204.

Rask-Andersen, M., Almén, M.S., and Schiöth, H.B. (2011). Trends in the exploitation of novel drug targets. Nat. Rev. Drug Discov. *10*, 579–590.

Russell, D.G., Cardona, P.J., Kim, M.J., Allain, S., and Altare, F. (2009). Foamy macrophages and the progression of the human tuberculosis granuloma. Nat. Immunol. *10*, 943–948.

Russell, D.G., VanderVen, B.C., Lee, W., Abramovitch, R.B., Kim, M.J., Homolka, S., Niemann, S., and Rohde, K.H. (2010). Mycobacterium tuberculosis wears what it eats. Cell Host Microbe *8*, 68–76.

Shin, D.M., Jeon, B.Y., Lee, H.M., Jin, H.S., Yuk, J.M., Song, C.H., Lee, S.H., Lee, Z.W., Cho, S.N., Kim, J.M., et al. (2010). Mycobacterium tuberculosis eis regulates autophagy, inflammation, and cell death through redox-dependent signaling. PLoS Pathog. *6*, e1001230.

Siess, E.A., Kientsch-Engel, R.I., and Wieland, O.H. (1982). Role of free oxaloacetate in ketogenesis. Derivation from the direct measurement of

mitochondrial [3-hydroxybutyrate]/[acetoacetate] ratio in hepatocytes. Eur. J. Biochem. *121*, 493–499.

Singh, R., Kaushik, S., Wang, Y., Xiang, Y., Novak, I., Komatsu, M., Tanaka, K., Cuervo, A.M., and Czaja, M.J. (2009). Autophagy regulates lipid metabolism. Nature *458*, 1131–1135.

Sørensen, A.L., Nagai, S., Houen, G., Andersen, P., and Andersen, A.B. (1995). Purification and characterization of a low-molecular-mass T-cell antigen secreted by Mycobacterium tuberculosis. Infect. Immun. *63*, 1710–1717.

Taggart, A.K., Kero, J., Gan, X., Cai, T.Q., Cheng, K., Ippolito, M., Ren, N., Kaplan, R., Wu, K., Wu, T.J., et al. (2005). (D)-beta-Hydroxybutyrate inhibits adipocyte lipolysis via the nicotinic acid receptor PUMA-G. J. Biol. Chem. *280*, 26649–26652.

Tansey, J.T., Sztalryd, C., Hlavin, E.M., Kimmel, A.R., and Londos, C. (2004). The central role of perilipin a in lipid metabolism and adipocyte lipolysis. IUBMB Life *56*, 379–385.

Tunaru, S., Kero, J., Schaub, A., Wufka, C., Blaukat, A., Pfeffer, K., and Offermanns, S. (2003). PUMA-G and HM74 are receptors for nicotinic acid and mediate its anti-lipolytic effect. Nat. Med. *9*, 352–355.

Wieland, O.H., Patzelt, C., and Löffler, G. (1972). Active and inactive forms of pyruvate dehydrogenase in rat liver. Effect of starvation and refeeding and of insulin treatment on pyruvate-dehydrogenase interconversion. Eur. J. Biochem. *26*, 426–433.

Xu, F.Y., Taylor, W.A., Hurd, J.A., and Hatch, G.M. (2003). Etomoxir mediates differential metabolic channeling of fatty acid and glycerol precursors into cardiolipin in H9c2 cells. J. Lipid Res. *44*, 415–423.